HHS Public Access

Author manuscript

J Neurooncol. Author manuscript; available in PMC 2016 September 01.

Published in final edited form as:

J Neurooncol. 2015 September ; 124(2): 175–183. doi:10.1007/s11060-015-1787-0.

Atypical Teratoid/Rhabdoid Tumor (ATRT) Arising from the 3rd Cranial Nerve in Infants: A Clinical-Radiological Entity?

Christopher C. Oh, MD[1,2], **Brent A. Orr, MD, PhD**[3], **Bruno Bernardi, MD**[4], **Maria Luisa Garré, MD**[5], **Andrea Rossi, MD**[6], **Lorenzo Figà-Talamanca, MD**[4], **Giles W. Robinson, MD**[7], and **Zoltán Patay, MD, PhD**[1]

[1]Department of Radiological Sciences, St. Jude Children's Research Hospital, Memphis, TN, USA

[2]Department of Radiology, University of Tennessee Health Sciences Center, Memphis, TN, USA

[3]Department of Pathology, St. Jude Children's Research Hospital, Memphis, TN, USA

[4]Department of Neuroradiology, Bambino Gesù Children's Hospital, Rome, Italy

[5]Neurooncology Unit, Istituto Giannina Gaslini, Genoa, Italy

[6]Neuroradiology Unit, Istituto Giannina Gaslini, Genoa, Italy

[7]Department of Oncology, St. Jude Children's Research Hospital, Memphis, TN, USA

Introduction

ATRT was originally described in 1996, and in 2000, it was added to the World Health Organization's brain tumor classification scheme as a distinct entity [1]. These embryonal tumors represent approximately 6.1% of all CNS neoplasms in the 0- to 14-y age group and are almost as common as primitive neuroectodermal tumor (PNET) and medulloblastoma in the 0- to 2-year age group. Rarely, ATRT may also be found in adults [2,3].

ATRTs have been described in virtually all CNS locations, including the cerebellopontine angle cisterns, meninges, cranial nerves, spinal canal [4–11], and extradural locations [12], as well as in locations outside the CNS (extra-renal rhabdoid tumors). Histologically, ATRTs demonstrate predominant rhabdoid tumor cells, with additional but variable components of neuroectodermal, epithelial, and mesenchymal origin [13]. However, several other tumors of embryonic origin may have a similar histologic appearance, presenting a potential diagnostic challenge [14].

Discoveries in molecular biology have demonstrated a characteristic loss of expression of the INI1 protein (also known as BAF47, SNF5) due to inactivation of the *SMARCB1* gene, which maps to the chromosomal locus 22q11.23 [15,16]. Detection of INI1 expression loss by immunohistochemistry is now required to make a formal histopathologic diagnosis of ATRT. Prior to the advent of SMARCB1 antibodies, ATRTs were commonly

Conflict of Interest

The authors disclose no conflict of interest with regards to the subject matter of this manuscript.

(approximately 50%) misdiagnosed, worsening the dismal prognosis of the disease. The 5-year survival rate of participants with correct initial diagnoses is more than 4 times higher (66.7%) than that of those with delayed diagnosis (15.0%) [17], making early and confident diagnosis of ATRT critical to augmenting survival.

Preoperatively, the diagnostic workup of patients with CNS tumors relies heavily on MRI, yet our current understanding of the MRI features of ATRTs is limited and derived from relatively small series [18–23]. ATRTs resemble PNETs or medulloblastomas by MRI, especially in their most critical T2 and DWI appearances [9,24–26]. Inevitably, a strong radiographic suggestion of a malignant tumor will lead to a diagnostic surgery. However, occasionally ATRTs have been found as small lesions and are not recognized as being potentially malignant; these lesions are then followed until progression, thus sacrificing the opportunity for early intervention.

Here, we present and describe three cases of these tumors arising from the CN III origin, all of which presented in patients within 6 months of birth, with isolated oculomotor nerve palsy and strikingly similar MRI characteristics. ATRTs originating from cranial nerves are rare and, to our knowledge, there has been only one previously published paper describing a single case of an ATRT arising from the origin of CN III [27]. The remarkable similarity of the 4 cases, however, suggests that the unique combination of the epidemiologic, neurologic, and MRI features in all of them define a highly suggestive clinical-radiological constellation, the recognition of which may enable earlier, confident diagnosis of ATRT and lead to earlier initiation of therapy.

Case Series

Our case series consists of 3 infants treated in 3 different pediatric hospitals. All of the patients underwent several MRI studies of the brain during the course of their disease. Imaging protocols varied, but all included T2-weighted imaging (T2WI), gadolinium contrast-enhanced T1-weighted imaging (GdT1WI), and diffusion-weighted imaging (DWI) sequences.

Retrospective review of the patients' medical files was conducted after approval and waiver-of-consent were obtained from the institutional research boards of all participating institutions. A coded data transfer agreement was signed between the institutions prior to the review of anonymized imaging data.

Patient 1

This white male patient, with unremarkable past medical and family history, initially presented to an outside hospital emergency department at the age of 5.5 months with right-sided ptosis and exotropia. Initial MRI examination was performed and was originally interpreted as being negative for disease. Shortly after presentation, the patient's dysconjugate gaze worsened, and he was referred to ophthalmology. This led to a review of the previously performed MRI, revealing a subtle signal abnormality of the anterior right cerebral peduncle, and a repeat MRI with contrast confirmed that a small 6-mm mass was

present at the right 3rd cranial nerve origin. (Figure 1 a–b) Routine 6-week follow-up of the lesion was recommended.

Symptoms quickly progressed to complete CN III palsy with emesis at feedings, and a second opinion was obtained. This led to a repeat MRI approximately 1 month after original presentation, which demonstrated interval growth. (Figure 1 c–f) Open surgical biopsy was performed, which revealed a thick fibrous lesion adherent to the CN III origin and adjacent neurovascular structures, precluding complete excision. Pathology findings were consistent with ATRT.

After surgery, the patient underwent four cycles of combination chemotherapy and subsequent proton beam therapy. Repeat MRI was obtained approximately 8 months after presentation, which showed interval progression. The patient died at the age of 14 months.

Patient 2

This female patient was born at term after an uneventful pregnancy and delivery, with unremarkable family history. The infant developed mild ptosis of the left eyelid around the 25th day after birth. Subsequently, the patient was seen by an ophthalmologist who diagnosed left oculomotor nerve palsy, prompting an MRI examination that revealed a small nodular lesion along the left 3rd cranial nerve, which was believed to be a schwannoma. (Figure 2 a–b)

A repeat MRI was performed after hospital admission of the patient at the age of 2 months, confirming the lesion's presence. Because of the age of the patient and the surgical risk associated with possible surgical removal of the lesion, further observation was decided upon. During the following month, the patient presented with seizures, abnormal eye movements, pallor, cyanosis, and hypotonia. The seizure episodes rapidly worsened, reaching 10–15 episodes per day. A follow-up MRI study of the patient at 14 weeks of age showed marked interval growth and extension towards the temporal lobe. (Figure 2 c–d) Leptomeningeal metastatic dissemination was also seen in both the supratentorial compartment and in the lumbosacral spinal canal.

A week later, the patient underwent surgery that achieved partial tumor removal only. The histopathologic diagnosis was atypical teratoid rhabdoid tumor.. One week after surgery, chemotherapy was initiated, but at the end of the 3rd cycle of the induction phase, the child presented with clinical and further radiological evidence of progression and died at the age of 5.5 months.

Patient 3

This female patient was born at term to non-consanguineous parents after an uncomplicated delivery. Her family history was unremarkable, and she had normal psychomotor development. At the age of 5 months, she presented with acute onset of ptosis of the right eye. Neurological examination revealed right 3rd cranial nerve palsy with ptosis, ophthalmoplegia, and non-reactive mydriasis.

The first MRI examination of the brain was performed within 48 hours after the clinical onset and revealed a small mass involving the right cerebral peduncle, with extension towards the interpeduncular cistern between the right posterior cerebral artery (PCA) and right superior cerebellar artery (SCA) along the cisternal course of the 3rd cranial nerve. The lesion was hypointense on T2WI, showed a low ADC, and avidly enhanced after IV contrast injection. (Figure 3 a–b)

Follow-up MRI of the brain was performed one week later and showed a mild increase of the exophytic component of the lesion. (Figure 3 c–d) A total-body computed tomography (CT) scan was performed a few days later and did not reveal any additional pathologic findings.

Another follow-up MRI examination of the brain was performed one month after the initial diagnostic imaging workup and revealed further increase of the primary lesion as well as perineural (along the 5th, 6th and 7th cranial nerves) and leptomeningeal (along the superior surface of the left cerebellar hemisphere) metastatic dissemination. (Figure 3 e–f)

The final MRI examination of the brain and spine occurred a few days later and showed additional seeding along the spinal cord, cauda equina roots, and hydrocephalus. (Figure 3 g–h) Another 10 days later, a surgical biopsy was performed on one of the cauda equina lesions; histopathologic findings, including immunohistochemistry, were consistent with ATRT.

The first two cerebrospinal fluid (CSF) cytology examinations (one at 2 days after onset of the clinical signs and symptoms and one at 2 weeks after onset) were normal, but the third CSF examination (at 6 weeks after onset) revealed the presence of neoplastic cells. The patient died at the age of 15 months.

Results

The parents of all of our infant patients initially sought medical attention for neurological signs and symptoms suggestive of oculomotor nerve palsy. The patients' demographic, imaging, and most relevant clinical data are summarized in Table 1.

On initial MR imaging, all 3 patients had a mass lesion arising from the CN III adjacent to the anterior aspect of one of the cerebral peduncles (2 right, 1 left) between the ipsilateral P1 and P2 segments of the posterior cerebral artery and the proximal segment of superior cerebellar artery. (Figure 1) In 2 patients (Patients 1 and 3), the lesions also involved the midbrain.

The masses were initially small (measuring 4–6 mm diameter) and were predominantly solid. The masses demonstrated variable but near-isointensity on T1-weighted images and iso- or relative hypointensity on T2-weighted images (Figures 1 and 2) with respect to adjacent brainstem parenchyma. Avid contrast enhancement was present in all of the cases. (Figures 1 and 3) ADC maps showed decreased signal within the tumors, consistent with restricted diffusion, suggesting increased cellular density. (Figures 1 and 3) In all cases, the

initial diagnosis was benign nerve sheath tumor; hence, monitoring was adopted as a management strategy.

Short-interval follow-up MRI showed an increase in size (Figures 1–3) with corresponding development of a few areas of cystic/necrotic changes. (Figure 2) No abdominal or renal masses to suggest synchronous malignant rhabdoid tumor were identified on ultrasonography or CT in the 2 patients (Patients 1 and 3) who underwent total body imaging workup.

No evidence of CSF dissemination of tumor was present on any of the initial MRI examinations, but all patients developed leptomeningeal seeding later during the course of the disease. (Figure 3) Leptomeningeal dissemination occurred as early as 23 days after initial MRI in one of our cases.

Open surgery was performed on all 3 of the participants. Histopathologic analysis led to a diagnosis of ATRT in each case. The sample from Patient 1 demonstrated significant atypia, with characteristic loss of SMARCB1 expression. (Figure 4 a) Additional immunostains in samples from that patient were positive for cytokeratin (CAM5.2), and Ki67/MIB-1 testing showed a high mitotic index. A comprehensive analysis of the patient's germline DNA derived from blood lymphocytes found no *SMARCB1* mutation, suggesting that the loss of SMARCB1 in the tumor was somatically acquired. In patient 2 hematoxylin-eosin stained sections showed hypercellular tumor dominated by rhabdoid cells with eccentric nuclei and eosinophilic cytoplasm. The specimen demonstrated loss of INI-1 immunoreactivity in tumor cells, but retained staining in the vascular elements. (Figure 4 b) The tumor was also immunoreactive for cytokeratin and smooth muscle actin. (not shown) In patient 3 the neoplasm consisted of medium sized cells with elongated and oval nuclei, prominent nucleoli, and eosinophilic cytoplasm. Tumor cells were arranged in a storiform and fascicular pattern. By immunohistochemistry, the tumor demonstrated loss of expression for the INI 1 protein in neoplastic cells but retained expression in the stromal elements. (Figure 4 c) Immunohistochemical analysis also demonstrated immunoreactivity for EMA (epithelial membrane antigen) and vimentin. (not shown)

After the diagnosis was established, all of the participants underwent treatment with combination chemotherapeutic regimens based on protocols within their respective institutions. One of the patients (Patient 1) underwent proton beam radiotherapy. Despite treatment, disease progression occurred rapidly, and all of the patients died within 10 months. Mean survival time after presentation was 7.5 months, with a range of 4.5 to 10 months.

Discussion

This case series presents 3 ATRTs in the unique location of the CN III (at or close to its origin from the midbrain) in infants presenting with isolated oculomotor nerve palsy. All were clinically identified early on due to focal neurological signs, but diagnosis was delayed due to failure to recognize the lesions as malignant. The imaging findings were nearly identical in each case and include the following: variable but near iso-intensity on T1-

weighted images, relative hypointensity on T2-weighted images, marked contrast enhancement, and intrinsic diffusion restriction. All of the masses were predominantly solid at presentation. As the tumors grew in size, T2-hyperintense cystic changes developed, consistent with areas of spontaneous or therapy-induced necrosis. Overall, these imaging findings are consistent with those found in ATRT in other, more common, CNS locations [6,9,10,12–14].

Outcomes in ATRT, even with extensive multimodal therapy, have historically been dismal; however, recent improvements in this area have come from therapies directed exclusively towards ATRT. This strategy of treating ATRT as an entity separate from other infantile brain tumors highlights the importance of making a timely and correct diagnosis. However, although diagnostic tests of tumor specimens have radically improved the ability to post-operatively identify ATRT, these tumors are not readily recognized preoperatively, especially when small. It is in this early stage of the disease that an intervention may be of greatest benefit.

Differential diagnostic considerations for a focal exophytic-appearing mass at or adjacent to the CN III origin are quite limited. Low-grade astrocytomas/gliomas can be avidly enhancing and have an exophytic appearance in the brainstem, but these are often located dorsally in the medulla oblongata and are also hyperintense on T2-weighted images with increased water diffusion [28,29].

In young infants, schwannomas involving CN III occur but are very rare in the absence of neurofibromatosis (NF) type 2 [30–32]. All 3 of our cases were initially misdiagnosed after imaging as being schwannomas (leading to short-term follow-up imaging rather than immediate, more-aggressive treatments) although none of our cases demonstrated additional lesions or clinical stigmata to suggest an underlying diagnosis of NF. A review of the recent literature shows that approximately 41 cases of isolated CN III schwannoma have been reported, of which 12 presented in the pediatric population [31]. However, none of those patients were younger than 6 months, and only 3 patients were younger than 3 years at diagnosis [32–34]. Although 2 of these 3 cases were later diagnosed as benign CN III schwannoma, one of these occurred in a 15-month-old patient who was eventually found histopathologically to have malignant schwannoma, which is now known as malignant peripheral nerve sheath tumor (MPNST) and whose location and certain imaging characteristics, including enhancement and restricted diffusion, are similar to those in our case series [34]. However, in that case, neither T2 images nor pathologic results were available for comparison or review. Also, MPNST affecting the cranial nerves is extremely rare, with approximately 19 cases present in the literature, and only 1 other case, in an adult, has ever been described to involve CN III [33,35,36]. Therefore, the aforementioned case is the only known oculomotor MPNST in a child [34].

Diffusion-weighted imaging is helpful in identifying both low-grade astrocytoma and benign schwannoma, which should not have the restricted diffusion seen in both ATRT and MPNST [37].

Due to the eloquent location of the tumors at the CN III origin, the resultant initial neuroophthalmological signs and symptoms were very focal and unequivocal and were remarkably similar to those reported previously [27]. The small size of the ATRTs in our series at initial diagnosis is in stark contrast to the sizes found in previous literature reports in which the average size of the largest tumor diameter was approximately 3.6–3.9 cm at presentation [14,38]. Additionally, other data suggest that gross total resection may lead to increased patient survival; hence, when possible, aggressive surgical resection should be performed [39,40]. Unfortunately, due to the brainstem location and adjacent vascular structures, total resection was not attempted or feasible, likely explaining the uniformly poor outcome in our cases.

In conclusion, ATRTs are commonly misdiagnosed initially, further exacerbating the dismal prognosis of the disease. Therefore, early, accurate diagnosis of this disease is critical. Awareness of the highly consistent and characteristic clinical and imaging pattern we have described here should facilitate such improvements in diagnosis. In an infant (typically < 6 months of age) presenting with isolated unilateral oculomotor nerve palsy, an enhancing tumor arising from the CN III adjacent to the midbrain that exhibits hypointensity on T2-weighted images and reduced water diffusion should be considered to be strongly suggestive of ATRT as a diagnosis. MPNST, though exceedingly rare (especially in infants and absent NF2), may appear similar and may have a better prognosis; underscoring the need for immediate biopsy, with excision if and when feasible.

Acknowledgements

The authors thank Dr. Fabio Facchetti, Brescia, Italy and Dr. Manila Antonelli, Department of Radiological, Oncological and Pathological Science, Sapienza University, Rome, Italy for generously providing histopathological images for Cases # 2 and #3; as well as Cherise M. Guess, PhD, ELS, for reviewing and editing the manuscript.

Funding

This work was supported in part by grant no. CA21765 from the National Cancer Institute and by the American Lebanese Syrian Associated Charities (ALSAC).

References

1. Rorke LB, Packer RJ, Biegel JA. Central nervous system atypical teratoid/rhabdoid tumors of infancy and childhood: definition of an entity. J Neurosurg. 1996; 85(1):56–65. [PubMed: 8683283]
2. Makuria AT, Rushing EJ, McGrail KM, Hartmann DP, Azumi N, Ozdemirli M. Atypical teratoid rhabdoid tumor (AT/RT) in adults: review of four cases. J Neurooncol. 2008; 88(3):321–330. [PubMed: 18369529]
3. Takahashi K, Nishihara H, Katoh M, Yoshinaga T, Mahabir R, Kanno H, Kimura T, Tanino M, Ikeda J, Sawamura Y, Nagashima K, Tanaka S. Case of atypical teratoid/rhabdoid tumor in an adult, with long survival. Brain Tumor Pathol. 2011; 28(1):71–76. [PubMed: 21181449]
4. Bing S. Face-lifting for a benign teratoid tumor of the nasiobregma. Plastic and reconstructive surgery. 1986; 78(1):120–121. [PubMed: 3725944]
5. Donovan DJ, Smith AB, Petermann GW. Atypical teratoid/rhabdoid tumor of the velum interpositum presenting as a spontaneous intraventricular hemorrhage in an infant: case report with long-term survival. Pediatr Neurosurg. 2006; 42(3):187–192. [PubMed: 16636624]
6. El-Nabbout B, Shbarou R, Glasier CM, Saad AG. Primary diffuse cerebral leptomeningeal atypical teratoid rhabdoid tumor: report of the first case. J Neurooncol. 2010; 98(3):431–434. [PubMed: 20020178]

7. Huddleston BJ, Sjostrom CM, Collins BT. Atypical teratoid/rhabdoid tumor involving cerebrospinal fluid: a case report. Acta Cytol. 2010; 54(5 Suppl):958–962. [PubMed: 21053577]
8. Takei H, Adesina AM, Mehta V, Powell SZ, Langford LA. Atypical teratoid/rhabdoid tumor of the pineal region in an adult. J Neurosurg. 2010; 113(2):374–379. [PubMed: 19911885]
9. Taneja AK, Reis F, Zanardi VA, Rogerio F, Queiroz LS. Meningeal presentation of an atypical teratoid/rhabdoid tumor. Neurol India. 2010; 58(4):681–682. [PubMed: 20739832]
10. Tanizaki Y, Oka H, Utsuki S, Shimizu S, Suzuki S, Fujii K. Atypical teratoid/rhabdoid tumor arising from the spinal cord--case report and review of the literature. Clin Neuropathol. 2006; 25(2):81–85. [PubMed: 16550741]
11. Verma A, Morriss C. Atypical teratoid/rhabdoid tumor of the optic nerve. Pediatr Radiol. 2008; 38(10):1117–1121. [PubMed: 18696060]
12. Kazan S, Goksu E, Mihci E, Gokhan G, Keser I, Gurer I. Primary atypical teratoid/rhabdoid tumor of the clival region. Case report. J Neurosurg. 2007; 106(4 Suppl):308–311. [PubMed: 17465367]
13. Athale UH, Duckworth J, Odame I, Barr R. Childhood atypical teratoid rhabdoid tumor of the central nervous system: a meta-analysis of observational studies. J Pediatr Hematol Oncol. 2009; 31(9):651–663. [PubMed: 19707161]
14. Strother D. Atypical teratoid rhabdoid tumors of childhood: diagnosis, treatment and challenges. Expert Rev Anticancer Ther. 2005; 5(5):907–915. [PubMed: 16221059]
15. Biegel JA. Molecular genetics of atypical teratoid/rhabdoid tumor. Neurosurg Focus. 2006; 20(1):E11. [PubMed: 16459991]
16. Lafay-Cousin L, Strother D. Current treatment approaches for infants with malignant central nervous system tumors. Oncologist. 2009; 14(4):433–444. [PubMed: 19342475]
17. Woehrer A, Slavc I, Waldhoer T, Heinzl H, Zielonke N, Czech T, Benesch M, Hainfellner JA, Haberler C, Austrian Brain Tumor R. Incidence of atypical teratoid/rhabdoid tumors in children: a population-based study by the Austrian Brain Tumor Registry, 1996–2006. Cancer. 2010; 116(24): 5725–5732. [PubMed: 20737418]
18. Arslanoglu A, Aygun N, Tekhtani D, Aronson L, Cohen K, Burger PC, Yousem DM. Imaging findings of CNS atypical teratoid/rhabdoid tumors. AJNR American journal of neuroradiology. 2004; 25(3):476–480. [PubMed: 15037475]
19. Biswas A, Goyal S, Puri T, Das P, Sarkar C, Julka PK, Bakhshi S, Rath GK. Atypical teratoid rhabdoid tumor of the brain: case series and review of literature. Child's nervous system : ChNS : official journal of the International Society for Pediatric Neurosurgery. 2009; 25(11):1495–1500.
20. Cheng YC, Lirng JF, Chang FC, Guo WY, Teng MM, Chang CY, Wong TT, Ho DM. Neuroradiological findings in atypical teratoid/rhabdoid tumor of the central nervous system. Acta Radiol. 2005; 46(1):89–96. [PubMed: 15841745]
21. Koral K, Gargan L, Bowers DC, Gimi B, Timmons CF, Weprin B, Rollins NK. Imaging characteristics of atypical teratoid-rhabdoid tumor in children compared with medulloblastoma. AJR Am J Roentgenol. 2008; 190(3):809–814. [PubMed: 18287456]
22. Lee YK, Choi CG, Lee JH. Atypical teratoid/rhabdoid tumor of the cerebellum: report of two infantile cases. AJNR American journal of neuroradiology. 2004; 25(3):481–483. [PubMed: 15037476]
23. Meyers SP, Khademian ZP, Biegel JA, Chuang SH, Korones DN, Zimmerman RA. Primary intracranial atypical teratoid/rhabdoid tumors of infancy and childhood: MRI features and patient outcomes. AJNR American journal of neuroradiology. 2006; 27(5):962–971. [PubMed: 16687525]
24. Niwa T, Aida N, Tanaka M, Okubo J, Sasano M, Shishikura A, Fujita K, Ito S, Tanaka Y, Kigasawa H. Diffusion-weighted imaging of an atypical teratoid/rhabdoid tumor of the cervical spine. Magnetic resonance in medical sciences : MRMS : an official journal of Japan Society of Magnetic Resonance in Medicine. 2009; 8(3):135–138.
25. Rumboldt Z, Camacho DL, Lake D, Welsh CT, Castillo M. Apparent diffusion coefficients for differentiation of cerebellar tumors in children. AJNR American journal of neuroradiology. 2006; 27(6):1362–1369. [PubMed: 16775298]
26. Yamashita Y, Kumabe T, Higano S, Watanabe M, Tominaga T. Minimum apparent diffusion coefficient is significantly correlated with cellularity in medulloblastomas. Neurol Res. 2009; 31(9):940–946. [PubMed: 19138469]

27. Wykoff CC, Lam BL, Brathwaite CD, Biegel JA, McKeown CA, Rosenblum MK, Allewelt HB, Sandberg DI. Atypical teratoid/rhabdoid tumor arising from the third cranial nerve. Journal of neuro-ophthalmology : the official journal of the North American Neuro-Ophthalmology Society. 2008; 28(3):207–211. [PubMed: 18769285]
28. Fisher PG, Breiter SN, Carson BS, Wharam MD, Williams JA, Weingart JD, Foer DR, Goldthwaite PT, Tihan T, Burger PC. A clinicopathologic reappraisal of brain stem tumor classification. Identification of pilocystic astrocytoma and fibrillary astrocytoma as distinct entities. Cancer. 2000; 89(7):1569–1576. [PubMed: 11013373]
29. Sridhar K, Sridhar R, Venkatprasanna G. Management of posterior fossa gliomas in children. Journal of pediatric neurosciences. 2011; 6(Suppl 1):S72–S77. [PubMed: 22069433]
30. Katsumata Y, Maehara T, Noda M, Shirouzu I. Neurinoma of the oculomotor nerve: CT and MR features. J Comput Assist Tomogr. 1990; 14(4):658–661. [PubMed: 2196295]
31. Niazi W, Boggan JE. Schwannoma of extraocular nerves: survey of literature and case report of an isolated third nerve schwannoma. Skull Base Surg. 1994; 4(4):219–226. [PubMed: 17171175]
32. Yang SS, Li ZJ, Liu X, Li Y, Li SF, Zhang HD. Pediatric isolated oculomotor nerve schwannoma: a new case report and literature review. Pediatr Neurol. 2013; 48(4):321–324. [PubMed: 23498569]
33. Chewning RH, Sasson AD, Jordan LC, Tamargo RJ, Gailloud P. Acute third cranial nerve palsy from a third cranial nerve schwannoma presenting as a saccular aneurysm on three-dimensional computed tomography angiography: case illustration. J Neurosurg. 2008; 108(5):1037. [PubMed: 18447727]
34. Sener RN. Malignant oculomotor schwannoma: diffusion MR imaging. Journal of neuroradiology Journal de neuroradiologie. 2006; 33(4):270–272. [PubMed: 17041535]
35. Santarius T, Chia HL, Xuereb JH, Kirollos RW. Sporadic malignant nerve sheath tumour of the oculomotor nerve. Acta Neurochir (Wien). 2007; 149(6):617–622. discussion 622. [PubMed: 17514351]
36. Scheithauer BW, Erdogan S, Rodriguez FJ, Burger PC, Woodruff JM, Kros JM, Gokden M, Spinner RJ. Malignant peripheral nerve sheath tumors of cranial nerves and intracranial contents: a clinicopathologic study of 17 cases. The American journal of surgical pathology. 2009; 33(3):325–338. [PubMed: 19065105]
37. Chhabra A, Thakkar RS, Andreisek G, Chalian M, Belzberg AJ, Blakeley J, Hoke A, Thawait GK, Eng J, Carrino JA. Anatomic MR imaging and functional diffusion tensor imaging of peripheral nerve tumors and tumorlike conditions. AJNR American journal of neuroradiology. 2013; 34(4): 802–807. [PubMed: 23124644]
38. Parwani AV, Stelow EB, Pambuccian SE, Burger PC, Ali SZ. Atypical teratoid/rhabdoid tumor of the brain: cytopathologic characteristics and differential diagnosis. Cancer. 2005; 105(2):65–70. [PubMed: 15690353]
39. Hilden JM, Meerbaum S, Burger P, Finlay J, Janss A, Scheithauer BW, Walter AW, Rorke LB, Biegel JA. Central nervous system atypical teratoid/rhabdoid tumor: results of therapy in children enrolled in a registry. Journal of clinical oncology : official journal of the American Society of Clinical Oncology. 2004; 22(14):2877–2884. [PubMed: 15254056]
40. Packer RJ, Biegel JA, Blaney S, Finlay J, Geyer JR, Heideman R, Hilden J, Janss AJ, Kun L, Vezina G, Rorke LB, Smith M. Atypical teratoid/rhabdoid tumor of the central nervous system: report on workshop. J Pediatr Hematol Oncol. 2002; 24(5):337–342. [PubMed: 12142780]

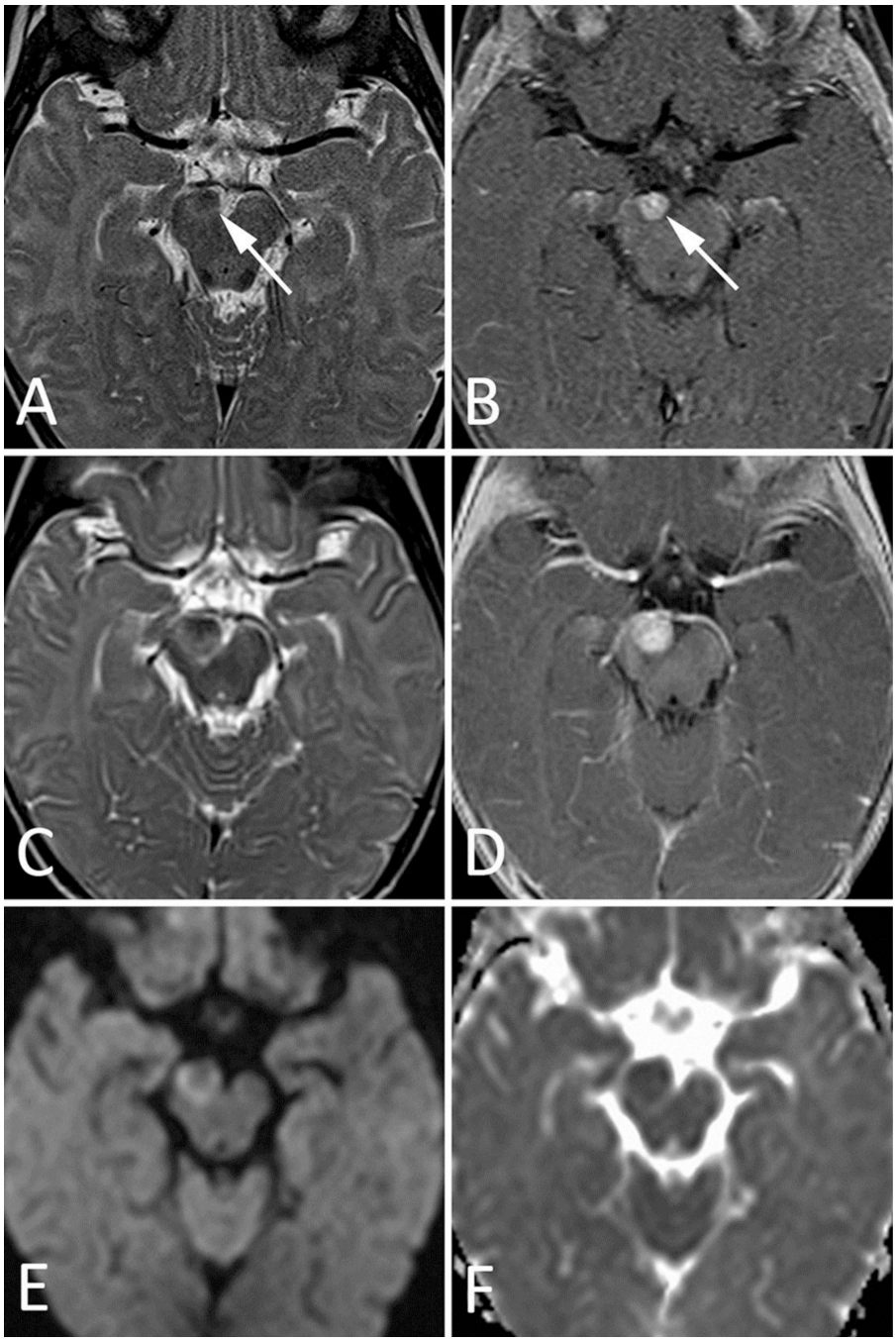

Fig 1. MRI Images of Patient 1

A–B. Initial MRI at presentation. a. Axial T2-weighted image through the level of the midbrain shows a small, solid, iso- to hypo-intense mass (arrow) at the expected location of the CN III origin in the anteromedial aspect of the right cerebral peduncle. b. Initial MRI at presentation. Axial postcontrast T1-weighted image shows slightly heterogenous but avid enhancement of the lesion (arrow).

C–F. Follow-up MRI 1 month after presentation. c. Axial T2-weighted image shows interval growth of the mass. Note the increased mass effect on the right P2 segment of the PCA,

which lies anterior to the mass. d. Axial postcontrast T1-weighted image clearly demonstrates interval increase in the size of the tumor. e. Axial DWI shows a relative increase in signal around the periphery of the lesion, with relative iso-intensity towards the center of the mass. f. Axial ADC map shows slightly decreased signal within the mass, confirming restricted water diffusion and suggesting internal hypercellularity.

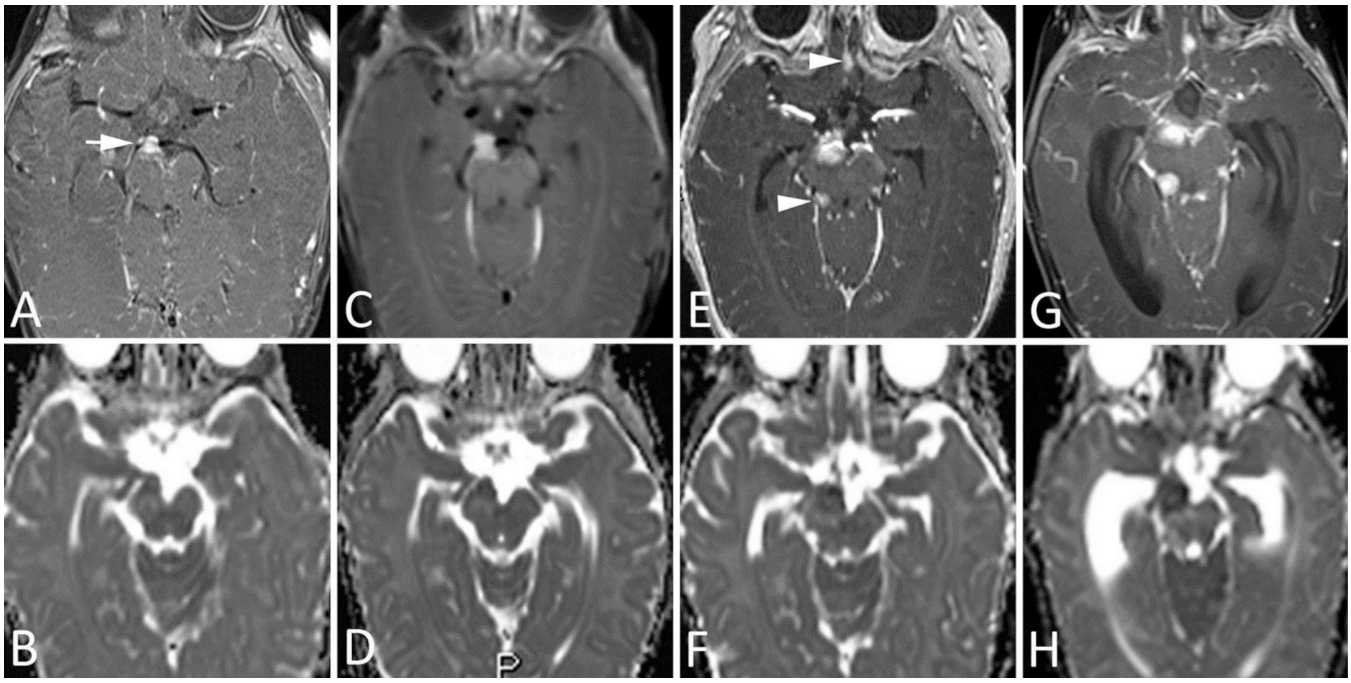

Fig 2. MRI Images of Patient 2

A–B. MRI of 2-month-old infant, performed 5 weeks after initial clinical presentation. a. Axial T2-weighted image shows a small, round, hypointense mass (arrow) just anterior to the left cerebral peduncle and involving the proximal segment of the cisternal portion of CN III. b. Coronal T2-weighted image shows the location of the mass (arrow) between the posterior cerebral artery and superior cerebellar artery.

C–D. Follow-up MRI taken 6 weeks after A and B (patient's age, 14 weeks). c. Axial T2-weighted image shows marked interval growth of the mass, with development of multiple internal areas of high T2 signal, likely representing foci of spontaneous necrosis. Note the interval extension of the mass towards the left temporal pole and the development of associated vasogenic edema. d. Coronal T2-weighted image shows increased splaying of the posterior cerebral and superior cerebellar arteries, indicating the mass effect. The presence of these adjacent neurovascular structures often preclude total resection.

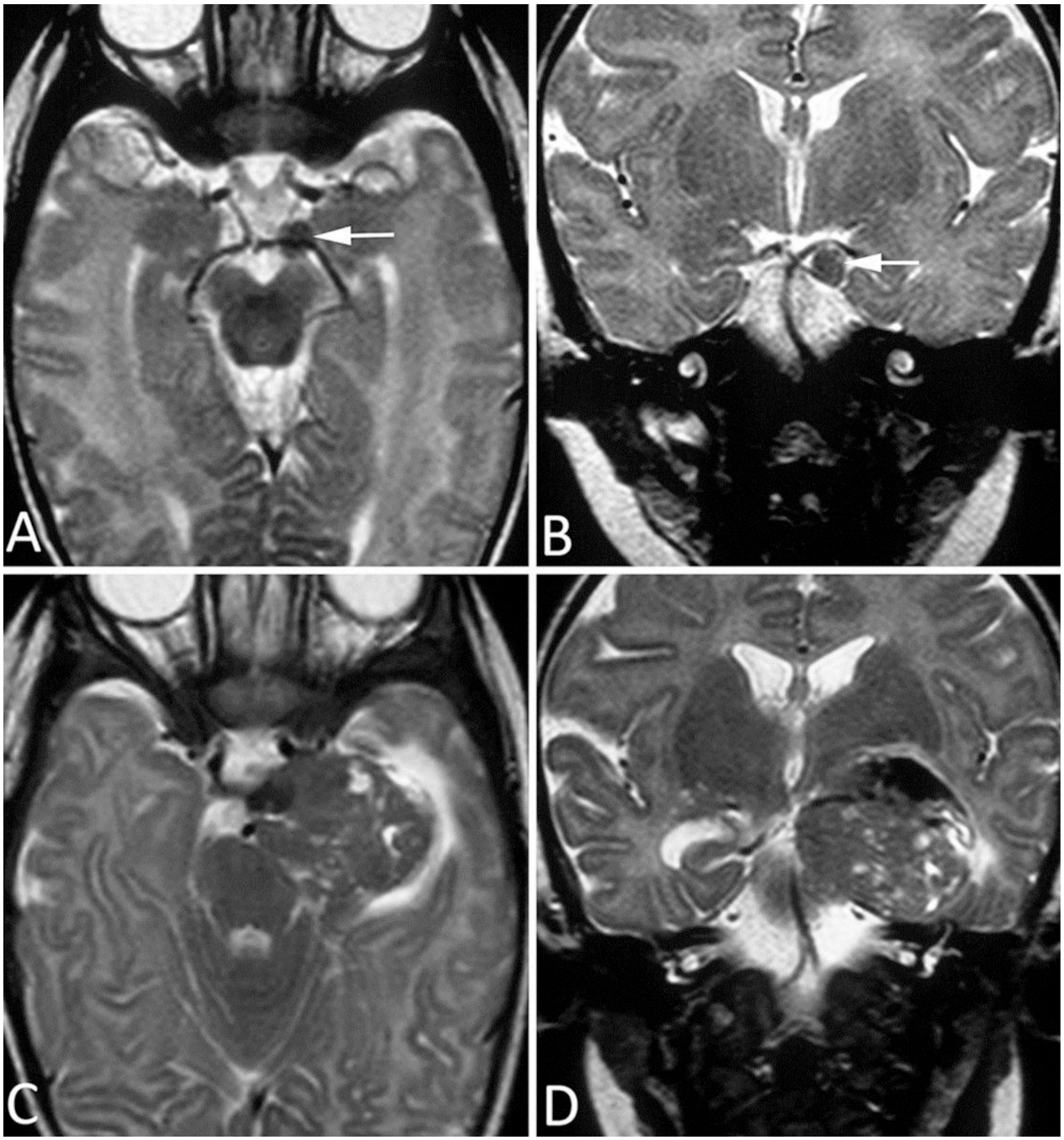

Fig 3. MRI Images of Patient 3

A–B. Initial MRI at presentation. a. Axial postcontrast T1-weighted image shows a solid, avidly enhancing lesion at the CN III origin, anterior to the right cerebral peduncle. b. Axial ADC image shows iso- to hypo-intense signal within the mass and moderately increased signal within adjacent brainstem parenchyma, indicating edema.

C–D. Follow-up MRI 1 week after presentation. c. Axial postcontrast T1-weighted image and (d.) precontrast ADC image show slight interval growth of the mass despite the very short follow-up interval.

E–F. Follow-up MRI 1 month after presentation. e. Axial postcontrast T1-weighted image and (f.) precontrast ADC image clearly demonstrate interval growth of the lesion, with two new remote foci of abnormal contrast enhancement—one in the right ambient cistern (arrowhead) and one in the olfactory region in the medline (arrowhead)—suggestive of leptomeningeal dissemination.

G–H. Follow-up MRI 5 weeks after presentation. g. Axial postcontrast T1-weighted image and (h.) precontrast ADC image show further interval growth of both the primary lesion and the metastatic deposit.

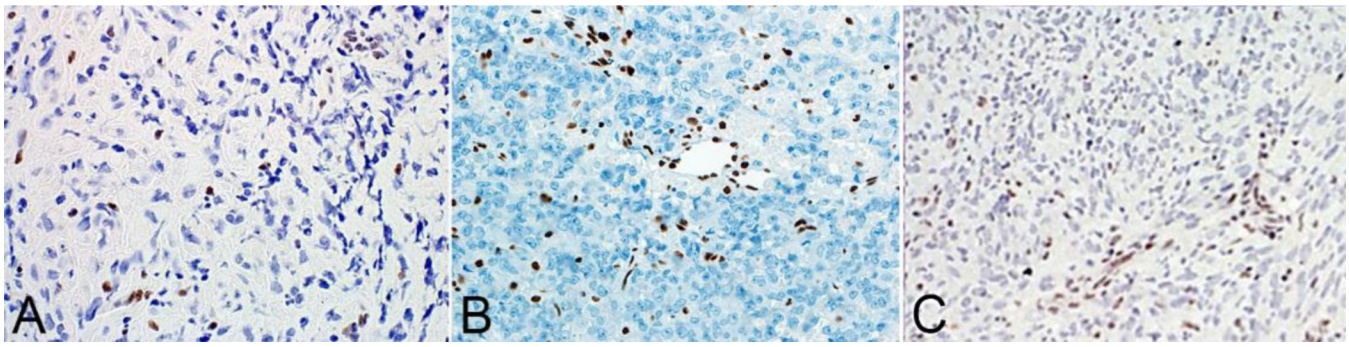

Fig 4. Immunihostochemistry of ATRT

In all 3 patients (A–C) immunostains to BAF47/INI1 show loss of staining in the tumor cells with retained immunostaining in the vessels.

Table 1

Demographic, MRI, and clinical data of our patients.

Patient No.	Sex	Age at diagnosis	Initial ophthalmologic signs at presentation	Side of lesion	Size of the lesion at diagnosis (largest diameter, mm)	MRI features	Surgery	Clinical evolution	Overall survival after presentation
1	M	5.5 mo	Ptosis, Exotropia, Dysconjugate gaze	R	6	T2WI GdT1WI ADC	Subtotal resection	Local tumor recurrence, leptomeningeal dissemination	8 mo
2	F	25 d	Ptosis	L	4	T2WI GdT1WI ADC	Subtotal resection	Local tumor recurrence, leptomeningeal dissemination	4.5 mo
3	F	5 mo	Ptosis, Non-reactive mydriasis	R	6	T2WI GdT1WI ADC	Subtotal resection	Local tumor recurrence, leptomeningeal dissemination	10 mo